Electronic Supplementary Material (ESI) for Journal of Materials Chemistry C.

Supporting Information

A facile strategy for fabricating self-healable, adhesive and highly sensitive flexible ionogel-based sensors

Yingxue Wu,[a] Wenxing Jiang,[a] Tianyu Zhao,[a] Jiadong Wang,[a] Xianhong Zhang,[a] Dong Chen[*a] Yuhong Ma,[a] and Wantai Yang[*ab]

[a] State Key Laboratory of Chemical Resource Engineering, College of Materials Science and Engineering, Beijing University of Chemical Technology, Beijing 100029, China

[b] Beijing Advanced Innovation Centre for Soft Matter Science and Engineering, Beijing 100029, China

Corresponding authors: yangwt@mail.buct.edu.cn, chendong@mail.buct.edu.cn

Preparation of MAH-2959. The synthetic route of the polymerizable photoinitiators MAH-2959 is shown in Scheme S1. Irgacure 2959 (5.0 g, 22.3 mmol), MAH (2.3 g, 23.5 mmol) and 4-dimethylaminopyridine (DMAP, 0.01g) as catalyst were dissolved in anhydrous tetrahydrofuran (20 mL), and the reaction system was then stirred at 70 °C for 8h in the dark. The orange viscous product MAH-2959 was obtained after the removal of THF by rotary evaporation.

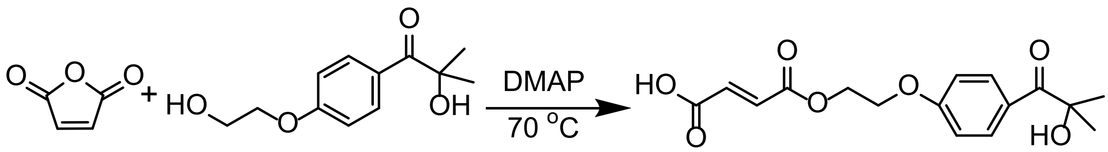

Scheme S1. The synthetic route of MAH-2959.

Characterization of MAH-2959. As shown in Fig. S1(a), the FTIR spectrum of MAH-2959 exhibited a typical C=O stretching vibration of ester groups at 1730 cm^{-1}. The proton nuclear magnetic resonance (^{1}H NMR) spectrum in Fig. S1(b) further demonstrated the successful formation of polymerizable photoinitiator MAH-2959.

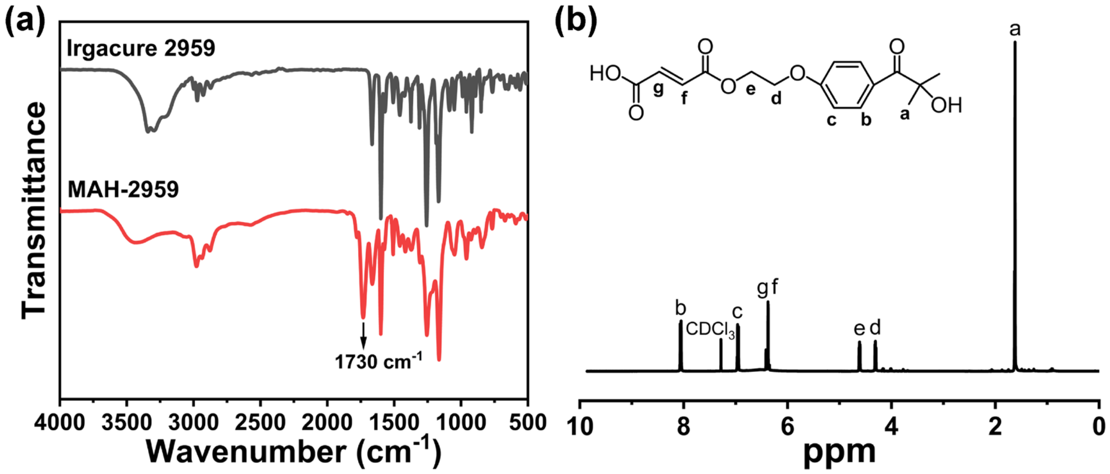

Fig. S1 (a) FTIR spectra of Irgacure 2959 and MAH-2959, (b) ^{1}H NMR spectrum of MAH-2959.

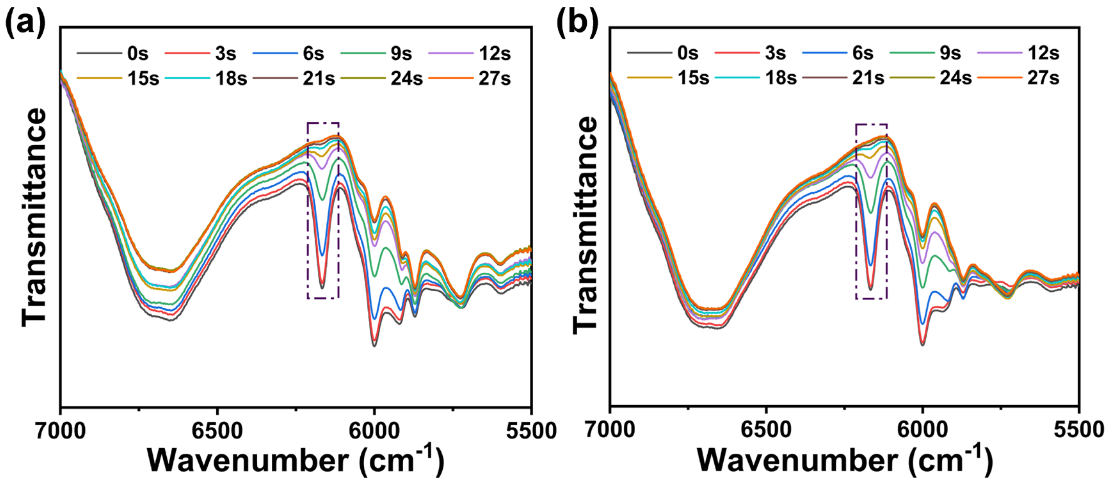

Fig. S2 FTIR spectra of PEI/PAA/DES ionogel prepared using (a) Irgacure 2959, (b) MAH-2959 in different reaction time.

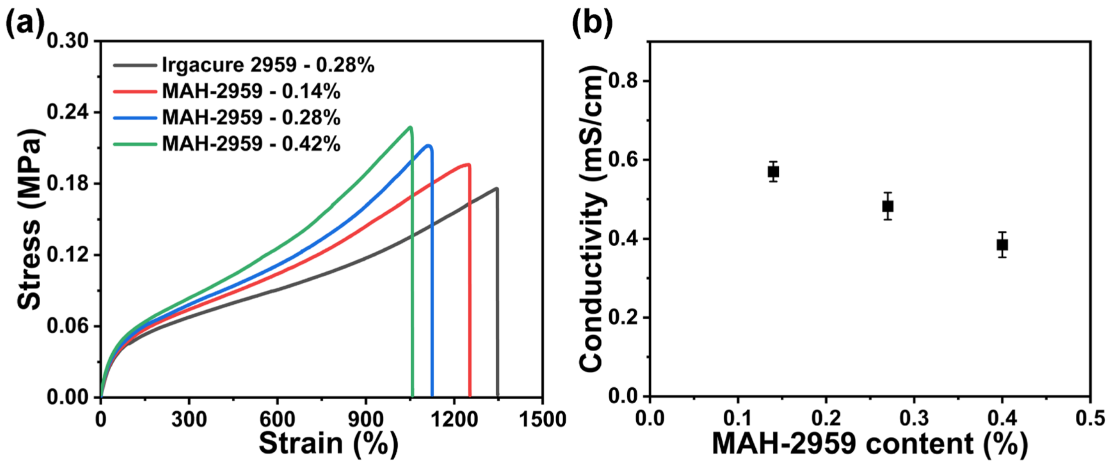

Fig. S3 (a)Tensile stress-strain curves and (b) conductivities of $PEI_{3.9}/PAA_9/DES_{72}$ ionogels prepared using different kind and content of photoinitiators.

Table S1. Compositions of $PEI_x/PAA_y/DES_z$ ionogels (0.28 wt%MAH-2959 relative to AA monomer, CCl-U:10.38g).

Sample	AA(g)	Mass fraction of AA in ionogel (wt%)	PEI(g)	Mass fraction of PEI in ionogel (wt%)	Mass ratio of PEI/DES ($\times 10^2$)	Mass ratio of PAA/PEI	Mass fraction of DES in ionogel (wt%)
$PEI_{3.2}/PAA_{11}/DES_{72}$	3.69	26	0.336	2.3	3.2	11	72
$PEI_{3.9}/PAA_{9}/DES_{72}$	3.63	25	0.403	2.8	3.9	9	72
$PEI_{4.9}/PAA_{7}/DES_{72}$	3.53	25	0.504	3.5	4.9	7	72
$PEI_{5.6}/PAA_{6}/DES_{72}$	3.45	24	0.576	4.0	5.6	6	72
$PEI_{4.7}/PAA_{9}/DES_{68}$	4.39	29	0.488	3.2	4.7	9	68
$PEI_{3.3}/PAA_{9}/DES_{75}$	3.11	23	0.345	2.5	3.3	9	75
$PEI_{2.8}/PAA_{9}/DES_{78}$	2.63	20	0.292	2.2	2.8	9	78
$PEI_{3.2}/PAA_{11}/DES_{72.4}$	3.63	25	0.330	2.3	3.2	11	72.4
$PEI_{5.0}/PAA_{7}/DES_{71.4}$	3.63	25	0.518	3.6	5.0	7	71.4
$PEI_{7.0}/PAA_{5}/DES_{70.4}$	3.63	25	0.725	4.9	7.0	5	70.4
$PEI_{3.9}/PAA_{11}/DES_{68.2}$	4.43	29	0.403	2.6	3.9	11	68.2
$PEI_{3.9}/PAA_{7}/DES_{76.3}$	2.82	21	0.403	3.0	3.9	7	76.3
$PEI_{3.9}/PAA_{5}/DES_{81.1}$	2.02	16	0.403	3.1	3.9	5	81.1

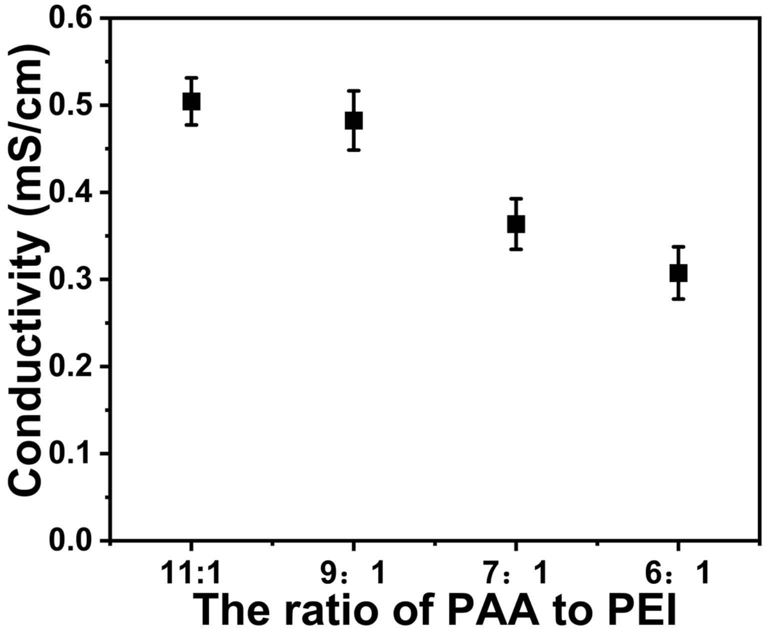

Fig. S4 Conductivities of $PEI_{3.2}/PAA_{11}/DES_{72}$, $PEI_{3.9}/PAA_{9}/DES_{72}$, $PEI_{4.9}/PAA_{7}/DES_{72}$ and $PEI_{5.6}/PAA_{6}/DES_{72}$.

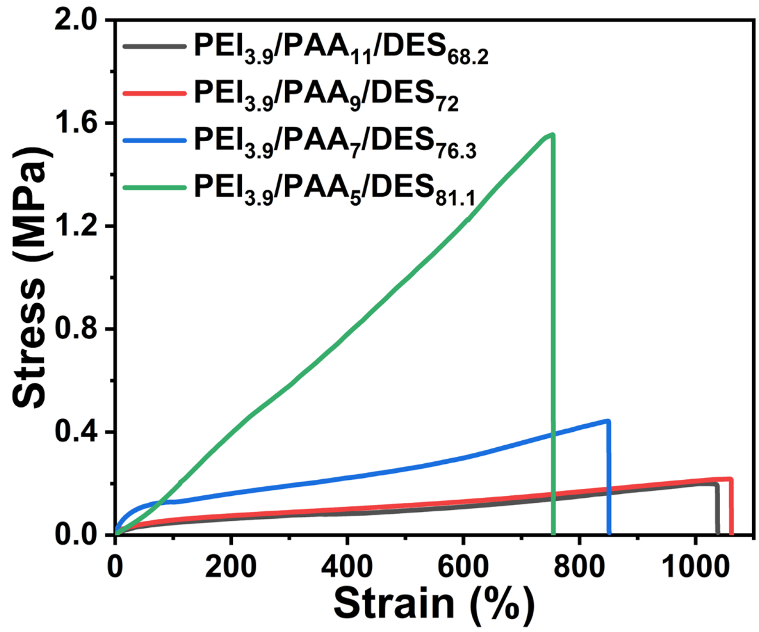

Fig. S5 Tensile stress-strain curves of $PEI_{3.9}/PAA_{11}/DES_{68.2}$, $PEI_{3.9}/PAA_{9}/DES_{72}$, $PEI_{3.9}/PAA_{7}/DES_{76.3}$ and $PEI_{3.9}/PAA_{5}/DES_{81.1}$.

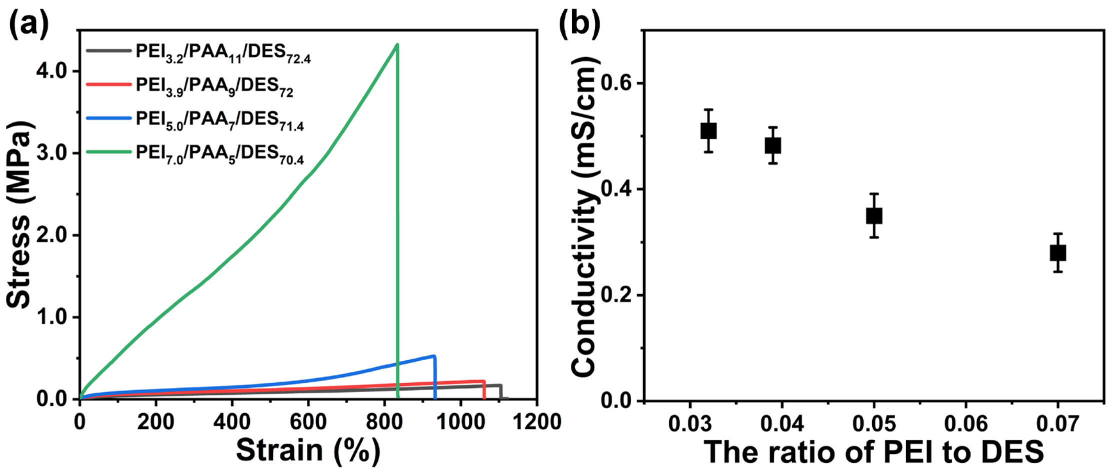

Fig. S6 (a) Tensile stress-strain curves and (b) conductivities of $PEI_{3.2}/PAA_{11}/DES_{72.4}$, $PEI_{3.9}/PAA_{9}/DES_{72}$, $PEI_{5.0}/PAA_{7}/DES_{71.4}$ and $PEI_{7.0}/PAA_{5}/DES_{70.4}$.

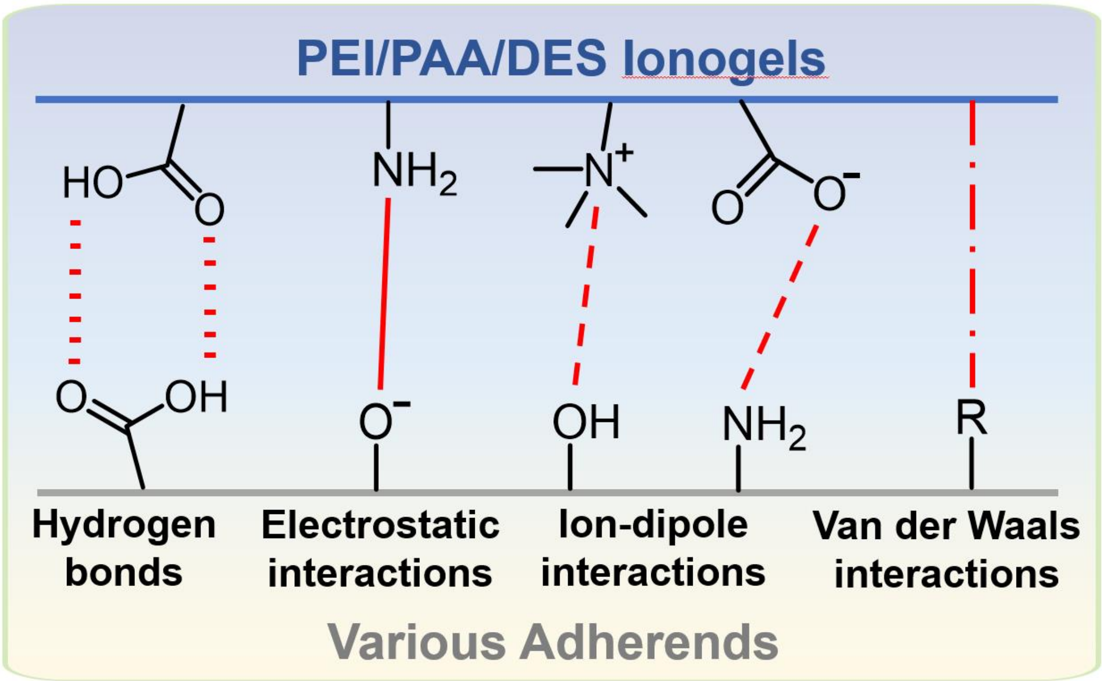

Fig. S7 The possible adhesive mechanisms between PEI/PAA/DES ionogels and various adherends.

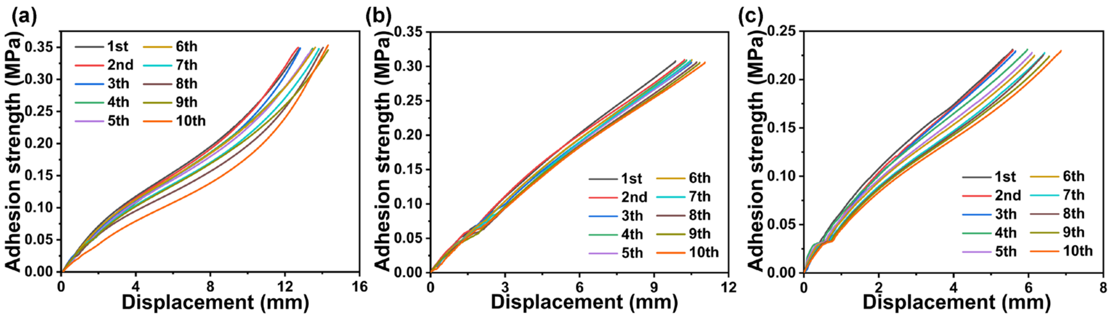

Fig. S8 The curves of adhesion strength vs displacement for $PEI_{3.9}/PAA_9/DES_{72}$ to (a) wood, (b) glass and (c) PVC during repeated adhesion progress.

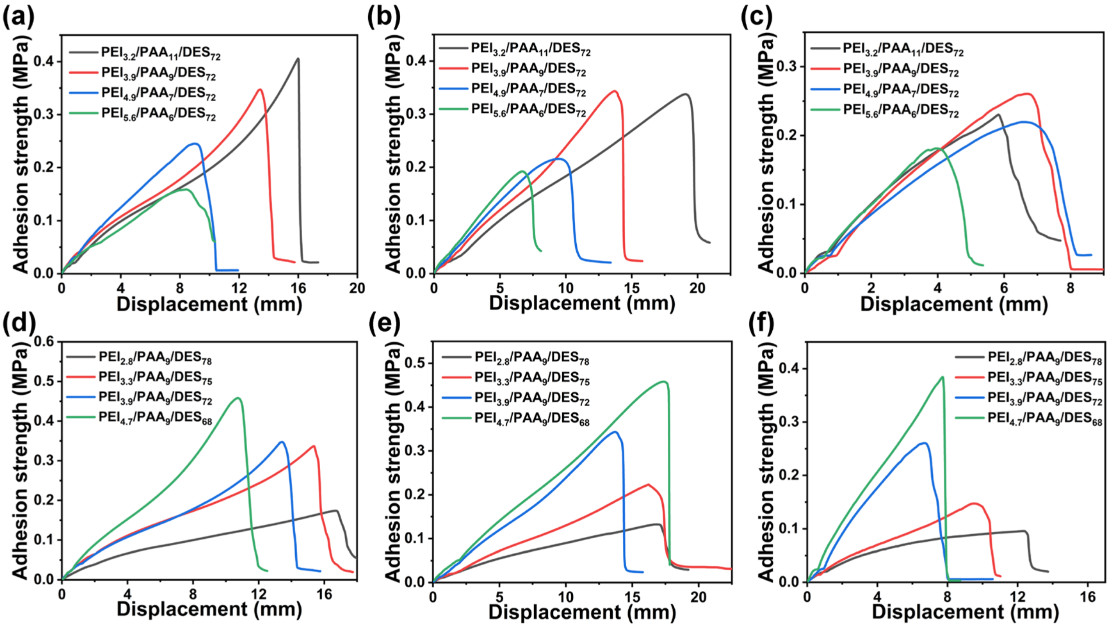

Fig. S9 Representative curves of adhesion strength vs displacement for $PEI_x/PAA_y/DES_{72}$ to (a) wood, (b) glass and (c) PVC with different ratio of PAA/PEI, Representative curves of adhesion strength vs displacement for $PEI_x/PAA_9/DES_z$ to (d) wood, (e) glass and (f) PVC with different polymer content.

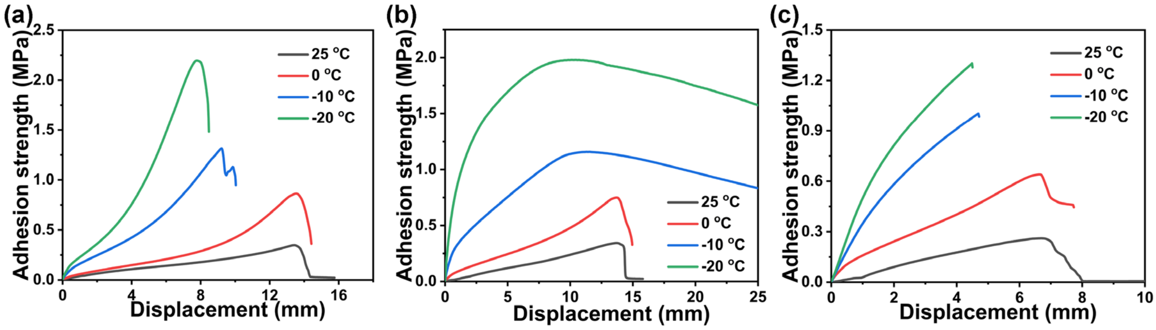

Fig. S10 Representative curves of adhesion strength vs displacement for $PEI_{3.9}/PAA_9/DES_{72}$ to (a) wood, (b) glass and (c) PVC at different temperature.

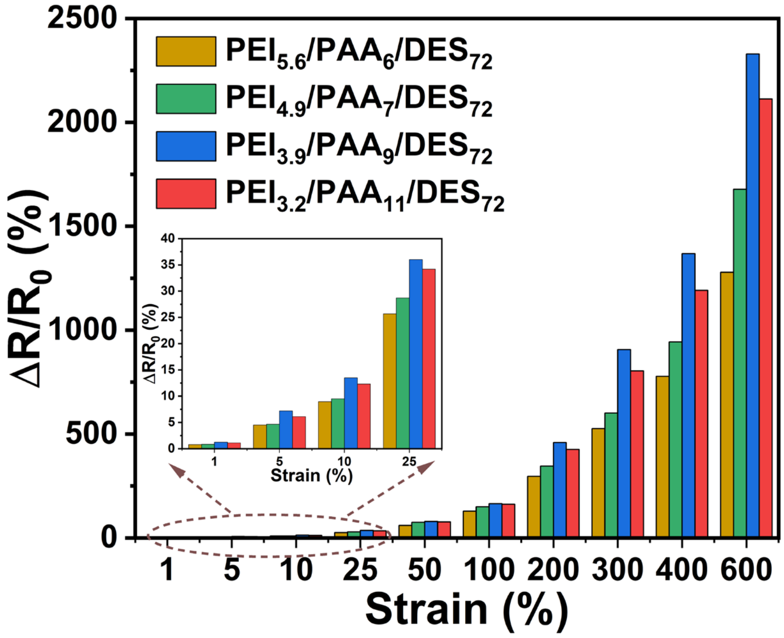

Fig. S11 Relative resistance changes of $PEI_x/PAA_y/DES_{72}$ ionogels with different ratio of PAA/PEI as a function of tensile strain.

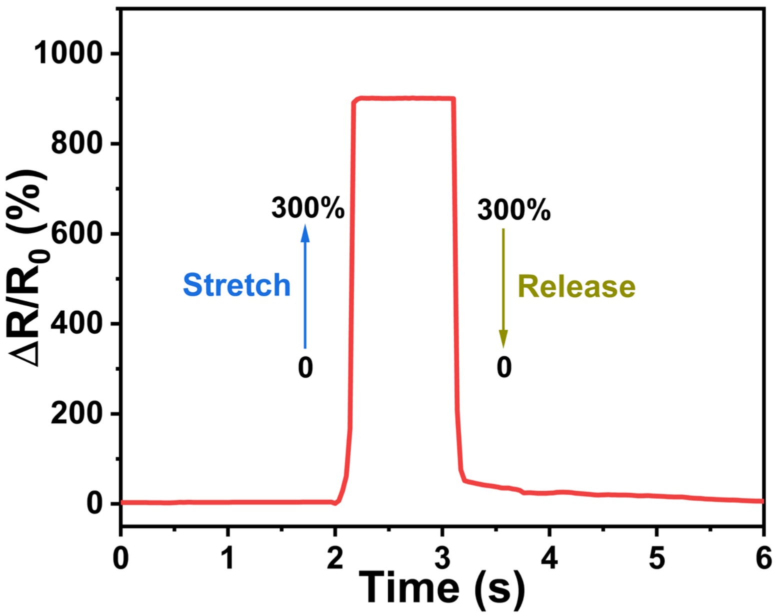

Fig. S12 Resistance changes of the $PEI_{3.9}/PAA_9/DES_{72}$ ionogel in the instantaneous loading-unloading process.

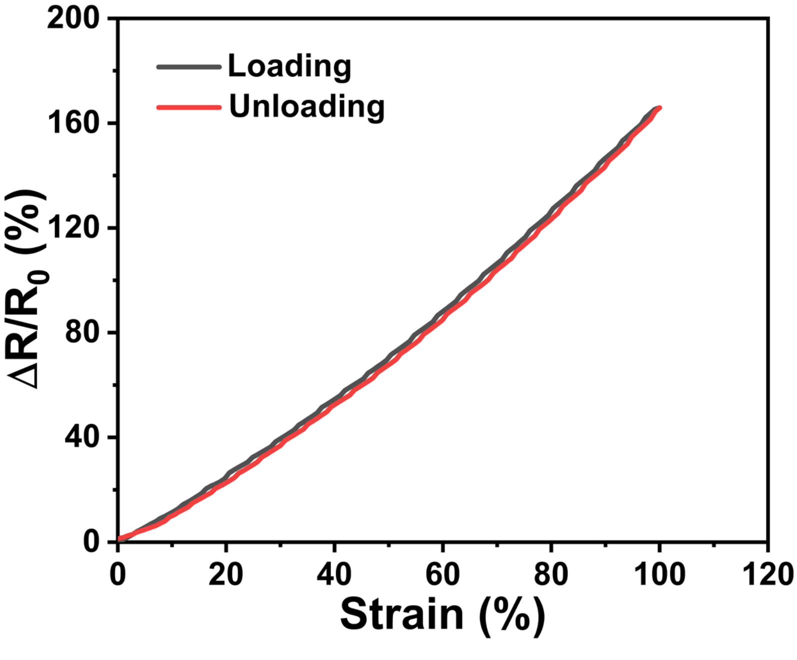

Fig. S13 Hysteresis curve of the $PEI_{3.9}/PAA_9/DES_{72}$ ionogel strain sensor at 100% strain.

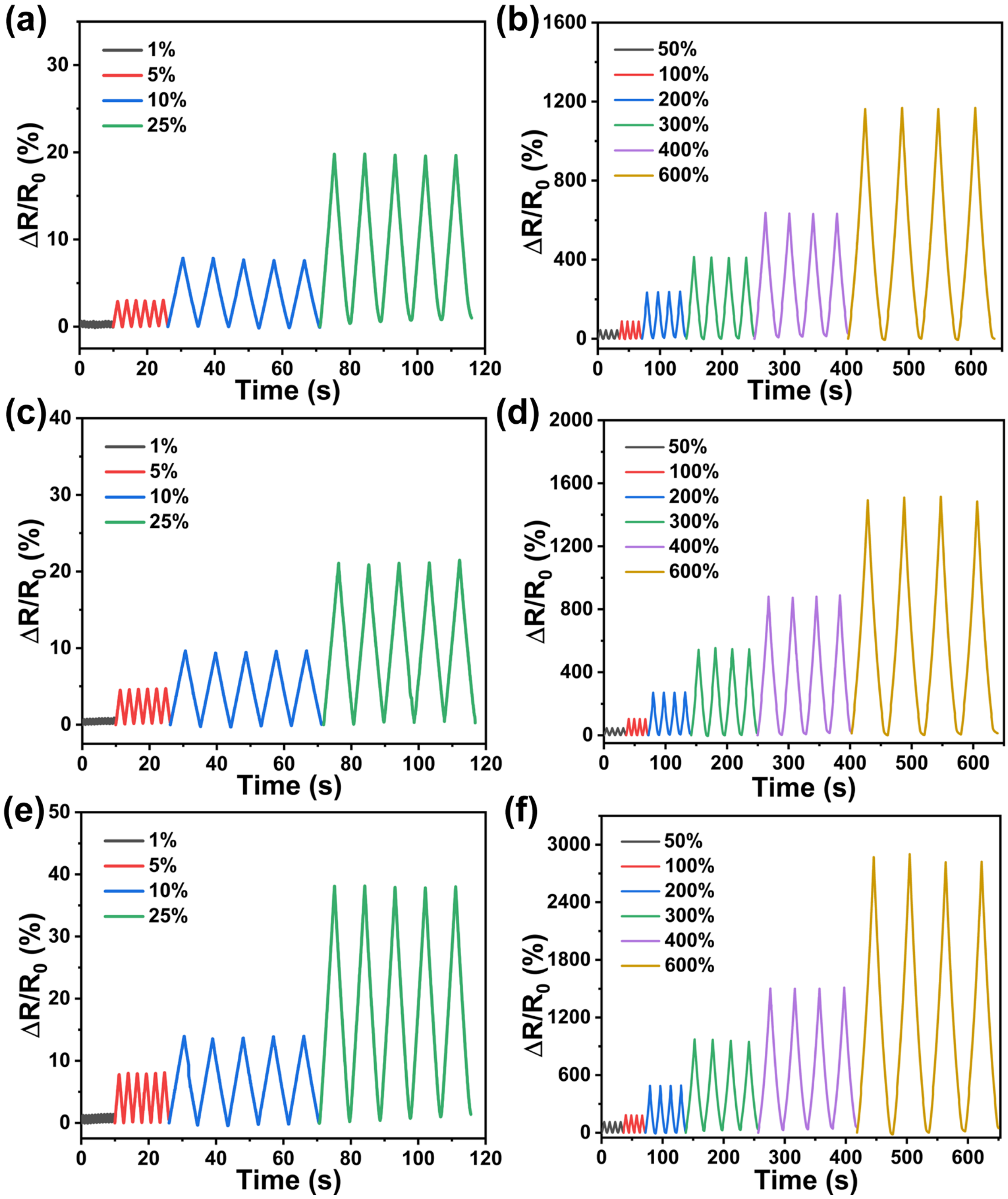

Fig. S14 Real-time monitoring of the relative resistance changes of (a-b) $PEI_{2.8}/PAA_9/DES_{78}$ ionogel, (c-d) $PEI_{3.3}/PAA_9/DES_{75}$ ionogel, and (e-f) $PEI_{4.7}/PAA_9/DES_{68}$ ionogel under different strains ranging from 1% to 600%.

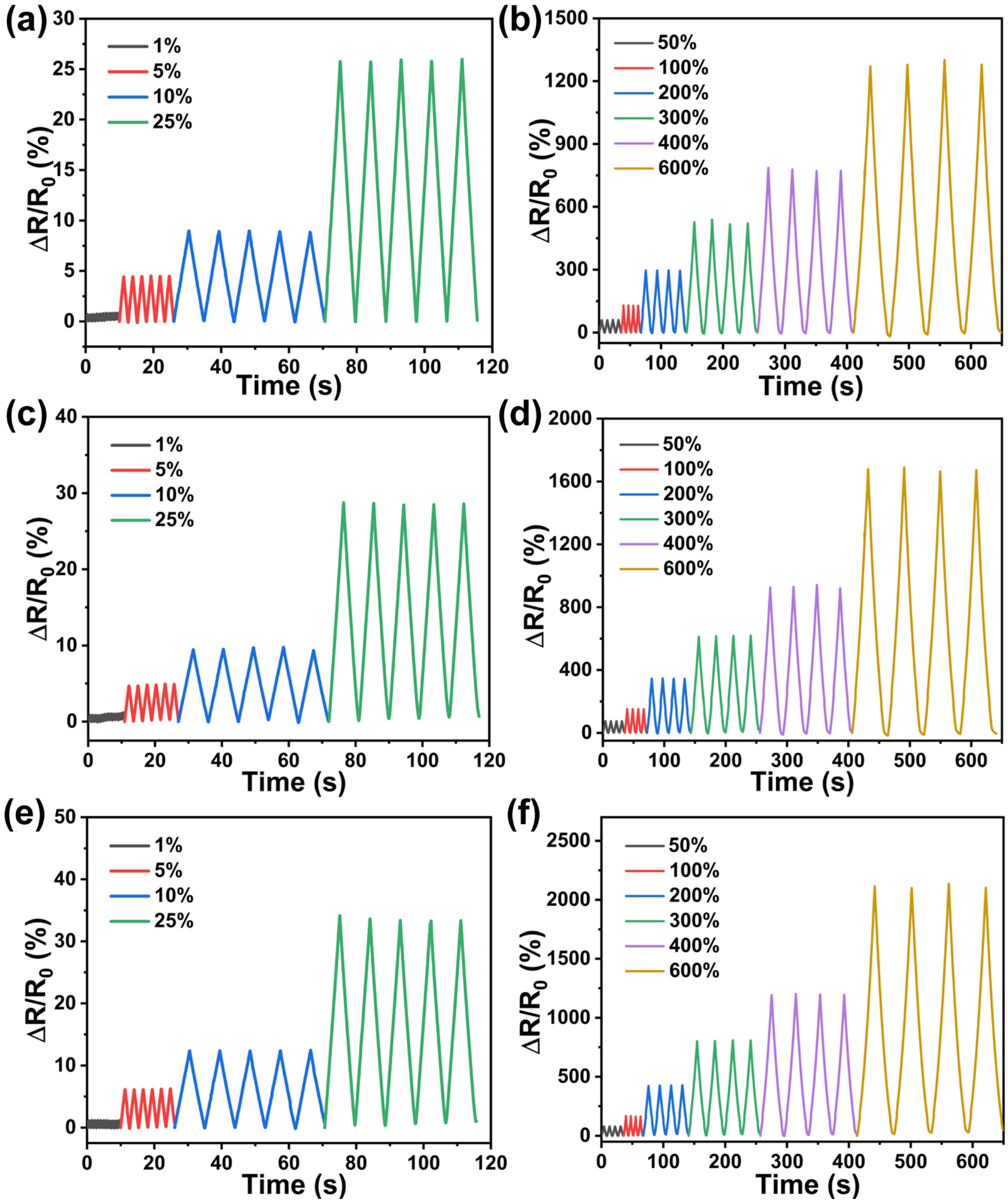

Fig. S15 Real-time monitoring of the relative resistance changes of (a-b) $PEI_{5.6}/PAA_6/DES_{72}$ ionogel, (c-d) $PEI_{4.9}/PAA_7/DES_{72}$ ionogel, and (e-f) $PEI_{3.2}/PAA_{11}/DES_{72}$ ionogel under different strains ranging from 1% to 600%.

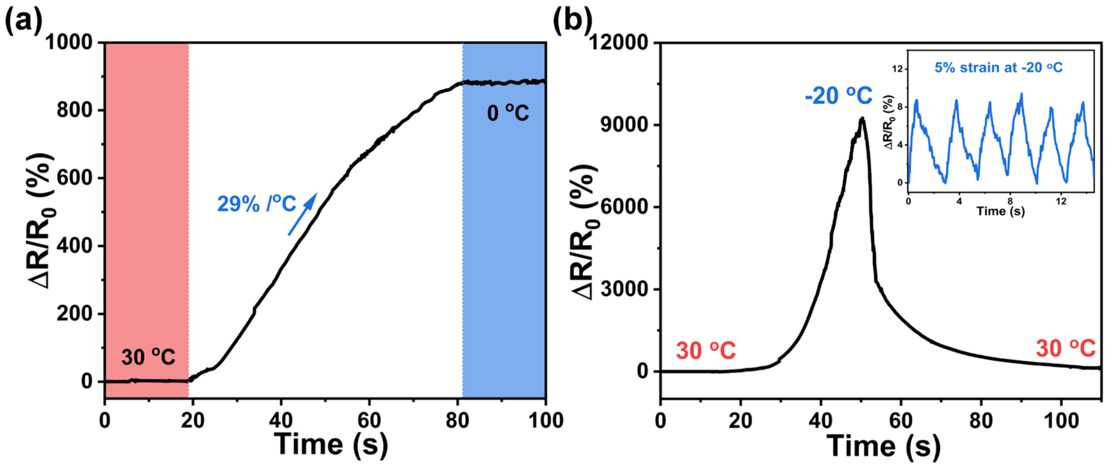

Fig. S16 (a) Resistance changes of the $PEI_{3.9}/PAA_9/DES_{72}$ ionogel for temperature detection (from 30 to 0 °C). (b) Resistance changes of the $PEI_{3.9}/PAA_9/DES_{72}$ ionogel during the cooling and heating process (between 30 and -20 °C). The inset displayed the real-time relative resistance changes of $PEI_{3.9}/PAA_9/DES_{72}$ under 5% strain at -20 °C.

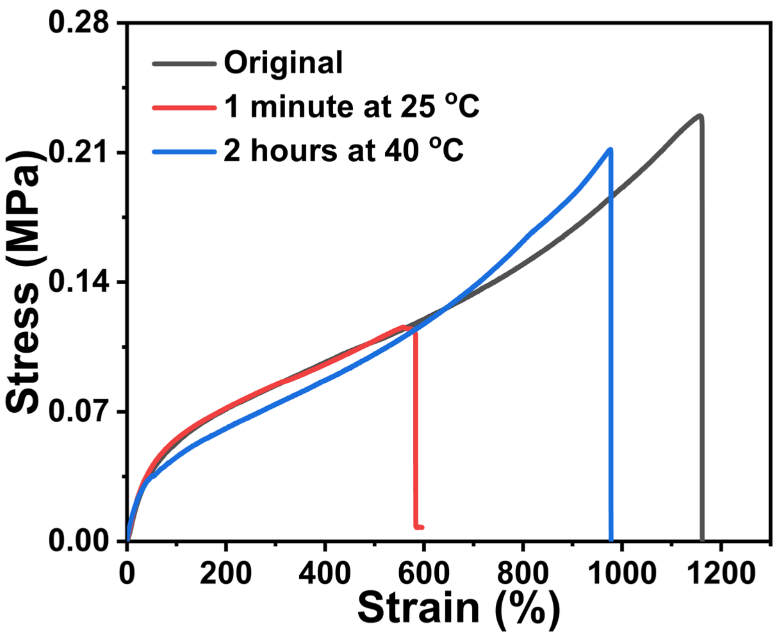

Fig. S17 Representative stress-strain curves of original and healed ionogel samples at different healing times and temperature.

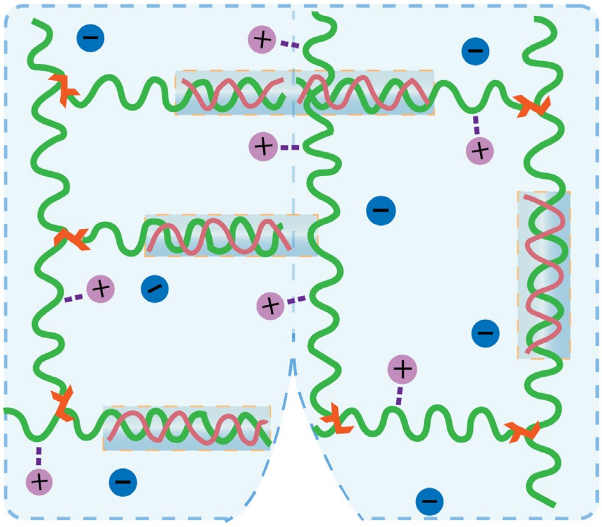

Fig. S18 The probable self-healing mechanism of the PEI/PAA/DES ionogels.

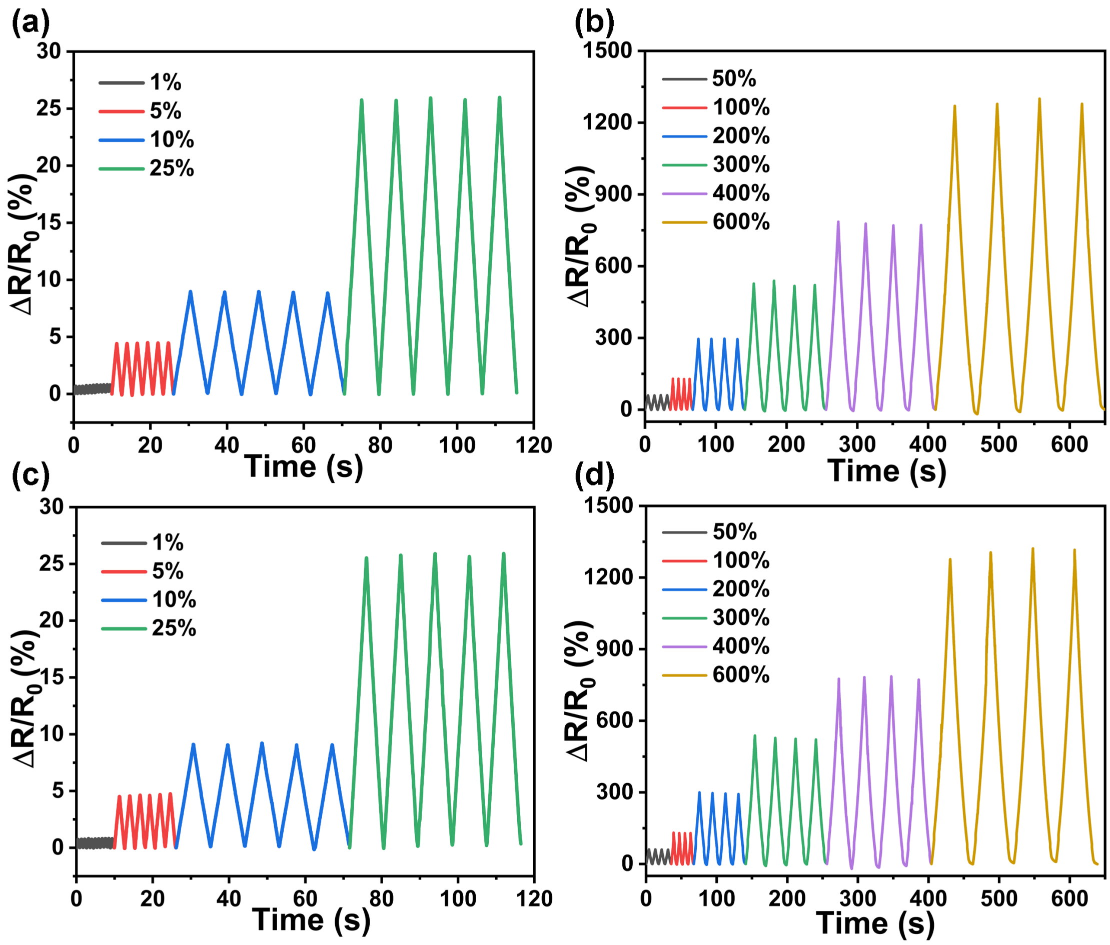

Fig. S19 Real-time monitoring of relative resistance of (a-b) $PEI_{5.6}/PAA_6/DES_{72}$ and (c-d) healed $PEI_{5.6}/PAA_6/DES_{72}$ under different strains ranging from 1% to 600%.

Table S2. A brief comparison of overall performance between $PEI_{3.9}/PAA_9/DES_{72}$-based strain sensor and representative ionogel-based sensors reported previously.

Ionogel-based sensor	GF	Maximum sensing range	Adhesive property (To glass)	Self-healing ability	Transmittance	Ref.
PEI/PAA/DES	4.68	600%	350 KPa	Yes	90%	This work
PVA/PVP/[EMIm][DCA]	1.85	400%	NA	Yes	85%	1
MMA/[VMIm][NTF_2]	2.3	300%	280 KPa	NA	NA	2
P(TFEA-co-AAm)/ [EMIM][TFSI]	1.85	600%	1000 N/m	Yes	92%	3
Chitosan/dextran–TA	0.44	400%	19.7 KPa	Yes	NA	4
PU/[DEIM][TFSI]	1.54	300%	NA	Yes	NA	5
PAA/[EMIM]Cl	1.6	200%	32 KPa	NA	90%	6
PU/[PMIM][EFSI]	2.14	200%	NA	Yes	95%	7
P(VDF-co-HFP)/ P(MMA-co-BMA)/[EMIM][TFSI]	1.62	150%	NA	NA	93%	8
P(ACMO/UA)/[EMIM][TFSI]	1.56	300%	NA	Yes	NA	9
PEA/[C_2mim][NTf_2]	1.83	200%	NA	NA	95%	10
PUU/ [EMIm][DCA]	4.64	300%	Yes	Yes	93%	11

[a] NA: not applicable

References

1. D. Weng, F. Xu, X. Li, S. Li, Y. Li and J. Sun, *ACS Appl. Mater. Interfaces*, 2020, **12**, 57477-57485.
2. J. Tie, Z. Mao, L. Zhang, Y. Zhong, X. Sui and H. Xu, *Compos. Pt. B-Eng.*, 2022, **232**, 109612.
3. L. Xu, Z. Huang, Z. Deng, Z. Du, T. L. Sun, Z.-H. Guo and K. Yue, *Adv. Mater.*, 2021, **33**, 2105306.
4. Y. Zhang, J. Xu and H. Wang, *RSC Adv.*, 2021, **11**, 37661-37666.
5. T. Li, Y. Wang, S. Li, X. Liu and J. Sun, *Adv. Mater.*, 2020, **32**, 2002706.
6. J. Sun, R. Li, G. Lu, Y. Yuan, X. Zhu and J. Nie, *J. Mater. Chem. C*, 2020, **8**, 8368-8373.
7. J. Xu, H. Wang, X. Du, X. Cheng, Z. Du and H. Wang, *Chem. Eng. J.*, 2021, **426**, 130724.
8. J. Lan, Y. Li, B. Yan, C. Yin, R. Ran and L.-Y. Shi, *ACS Appl. Mater. Interfaces*, 2020, **12**, 37597-37606.
9. M. Zhang, X. Tao, R. Yu, Y. He, X. Li, X. Chen and W. Huang, *J. Mater. Chem. A*, 2022, **10**, 12005-12015.
10. Z. Cao, H. Liu and L. Jiang, *Mater. Horizons*, 2020, **7**, 912-918.
11. L. Chen and M. Guo, *ACS Appl. Mater. Interfaces*, 2021, **13**, 25365-25373.